Broadband saturable absorption and ultrafast carrier dynamics of gold nanoparticles

JIA LIU, HAILONG YU, SHUANG YANG, YACHEN GAO*
Electronic Engineering College, Heilongjiang University, Harbin, 150080, China

Optical nonlinear absorption and ultrafast carrier dynamics in 20 nm gold nanoparticles (NPs) were studied using open-aperture (OA) Z-scan technique and transient absorption spectroscopy. In the OA Z-scan, the gold NPs were observed to exhibit broadband saturable absorption (SA) in the range of 475 ~ 600 nm under different excitation wavelengths and energies, and the SA was energy-dependent. The underlying physical mechanism was explained in terms of ground-state bleaching, and relevant optical parameters of the nonlinear absorption were obtained via theoretical analysis. In addition, the ultrafast dynamics of gold NPs were studied in the resonant and non-resonant regions using femtosecond pump-probe technology. It was observed that, for a certain pump fluence, the decay time becomes increase with the extension of the probe wavelength. These results indicate that gold nanomaterials have potential applications and significant value in laser Q-tuning and mode-locking.

(Received June 27, 2024; accepted December 2, 2024)

Keywords: Gold nanoparticles, Carrier dynamics, Broadband, Optical nonlinear absorption, Saturable absorption

1. Introduction

In recent years, significant progress has been made in the design, synthesis, and application of nanostructured materials, providing strong support for the development and application of nanotechnology [1]. Among these materials, noble metal nanoparticles (NPs), including gold NPs, have received significant attention. Gold NPs are usually present as nanostars [2], nanospheres [3], gold nanorods [4, 5], nanoshells [6], and bipyramidal structures [7], which have good chemical and thermal stability, as well as large nonlinear optical (NLO) properties and ultrafast response times [8-11]. Their susceptibility to surface plasmon resonance (SPR) [12] in the visible region makes them potential applications in photocatalytic, bio-detection, and optoelectronics [13-19]. In 2022, Peckus et al. synthesized gold nanoparticles with controllable shape, size, and dispersion, and showed by transient absorption (TA) spectroscopy, that the ultrafast response of gold NPs depends on the size of nanoparticles at high emission intensities [20]. Previous investigations imply that the optical nonlinearity of metal nanomaterials is affected by size and shape [21, 22]. However, due to limitation in experimental conditions, most of the previous studies are conducted using a single specific wavelength and pulse width [23]. In 2021, Fathima et al. reported the nonlinear optics study of laser-induced synthesis of gold NPs, using a 532 nm laser of a Q-switched Nd:YAG laser for the open-aperture (OA) Z-scan. Under the excitation of different energies, gold NPs were found to exhibit strong reverse saturation absorption [24].

In this work, we use the OA Z-scan (with continuously adjustable wavelength) and pump-probe (utilizing wider pulse width) technologies to study the non-linear absorption and ultra-fast response mechanisms of gold NPs in more detail. The absorption process of gold NPs is studied in depth and discussed in detail in terms of NLO absorption at different excitation wavelengths and energies. Correspondingly, we obtained the saturation light intensity, nonlinear absorption coefficient, response times of gold NPs. TA spectra were measured using different probe wavelengths, which helped us to understand the decay channels of gold NPs at different energy levels.

2. Samples and experiments

The gold NPs used in this experiment were synthesized according to the methods described in the references [25]. Specifically, prepare 85 ml of distilled water, add 5 mg of chloroauric acid solution to it stir vigorously. Then 5 ml of 1% sodium citrate solution was added at boiling temperature, resulting in the color transformation from grey to purple, red and finally deep red. The gold NPs were obtained after the colloidal solution had returned to room temperature. The morphology and size distribution of the gold NPs were characterized using scanning electron microscopy (SEM).

The linear absorption spectrum was measured with a UV-Visible spectrophotometer (TU-1901, Beijing Purkinje General Instrument Co., Ltd).

The OA Z-scan technique was used to study the nonlinear absorption characteristics of gold NPs [23]. The nanosecond Nd:YAG laser (Surelite II, Continuum, Santa Clara, CA, USA) was used as the light source, which was coupled to an optical parametric oscillator (APE OPO, Continuum) with an output pulse width of 6 ns and a repetition frequency of 10 Hz. The sample was positioned in a 2 mm cuvette, and the laser beam was focused on the cuvette. The incident and transmitted laser energies are detected by two energy meters (EPM 2000, Coherent) and recorded on a computer.

The ultrafast dynamics process of gold NPs was measured by pump-probe method [26]. An amplified femtosecond Ti: sapphire laser system generates a laser beam with a repetition rate of 1 kHz. The amplified can provide 130 fs, 800 nm pulses. In this case, a pulsed laser beam is frequency-doubled by a BBO crystal to produce 400 nm excitation light. Another pulse of laser light is focused on a sapphire crystal, generating continuous white light in the range of 420-750 nm as probe and reference light. The probe laser passes through the sample, where the signal is collected by a monochromator. Detection is carried out by a silicon photodetector, and fed into a lock-in amplifier. Finally, the data is observed through a computer.

3. Results and discussions

As shown in Fig. 1(a), it can be clearly observed from the SEM images that the gold NPs have a spherical morphology and they have a diameter of about 20 nm, and the NPs of different sizes have some unique properties. As shown in Fig. 1(b), the absorption spectrum that the gold NPs were measured with a UV-vis spectrophotometer. A strong absorption peak can be clearly observed at about 525 nm, which is indeed a typical feature of SPR of gold NPs. SPR is a phenomenon in which the free electrons in gold NPs undergo collective oscillations in the presence of an incident light electromagnetic field. The position of the SPR peak of gold NPs is influenced by its size, shape, dielectric environment and composition.

In order to gain a deeper understanding of the nonlinear absorption process in gold NPs, performing OA Z-scan measurements is a very effective method. This technique allows us to study the optical response of materials under untense laser irradiation, especially those processes related to nonlinear absorption. In the OA Z-scan experiments, the laser excitation energies were selected as 750, 1080 and 1380 μJ. The wavelength range of the laser was adjusted across a broad spectral range from 475 to 600 nm. As depicted in Fig. 2, following data processing and comparison, four representative curves were selected from each group of energy, and the samples were excited at 475, 525, 550, and 600 nm.

In Fig. 2, the saturated absorption (SA) behavior of gold NPs at four different excitation wavelengths is given. The SA is a NLO phenomenon in which the material has a higher transmittance at the focal point (z=0). When the excitation wavelength is the same and the incident light gradually increases, the peak of the SA curve also increases, indicating a stronger SA effect. At the same incident energy, gold NPs exhibit SA at all four wavelengths. By comparison, it can be concluded that the strongest absorption occurs at 525 nm. The physical mechanism is explained as follows: when the laser energy is low, the electrons in the ground state (GS) are pumped to the excited state (ES). As the laser energy increases, more GS electrons are pumped to the ES, inducing bleaching of the GS plasma [27]. Therefore, in the OA Z-scan, increased incident light leads to lower GS absorption of the sample, which cause the SA in the gold NPs.

Based on the above results, there is only SA observed in the sample. The nonlinear absorption coefficient is an important parameter used in NLO to characterize the change in absorption properties of a material under intense light and can be defined [23] as:

$$\alpha(I)=\frac{\alpha_0}{1+(I/I_S)} \tag{1}$$

where α_0 is the linear absorption coefficient of the material, I is the incident light intensity, I_s is the saturation intensity. We can express I as follows:

$$I=\frac{I_0}{1+z^2/z_0^2} \tag{2}$$

I_0 is the peak intensity at the focus, z is the sample from the focus (z=0), and z_0 is the Rayleigh diffraction length.

Since the thickness of the sample in the test is small relative to the length of the z_0, the influence on the results can be ignored. Therefore, we approximate the cuvette thickness L=2 mm in the above equation, so that the transmittance of the sample can be expressed as:

$$T(z)=1-\alpha(I)L \tag{3}$$

According to equations (1) - (3), the normalized transmittance can be considered as follows:

$$T(z)=1-\alpha(I)L=1-\frac{\alpha_0 L}{1+\dfrac{I_0}{\left(1+z^2/z_0^2\right)I_s}} \tag{4}$$

According to the above equations, the NLO parameters shown in Table 1 can be obtained, and their theoretical fitting curves are depicted as solid lines in

Figs. 2(a-d).

Because the saturation intensity is the largest at the linear absorption peak, we use dotted lines to represent the saturated light intensity in Fig. 3, where the linear absorption spectrum of 20 nm gold NPs is shown by solid lines. By comparing the solid and dotted lines, we can visualize the strong dependence of the saturated light intensity on the excitation wavelength and SPR.

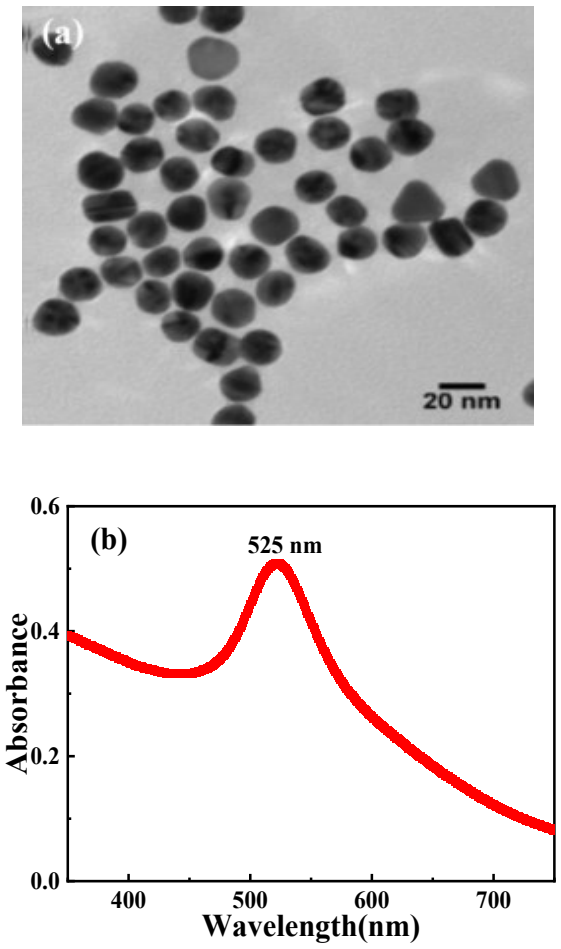

Fig. 1. (a) SEM images and (b) UV-vis spectra of 20 nm diameter gold NPs

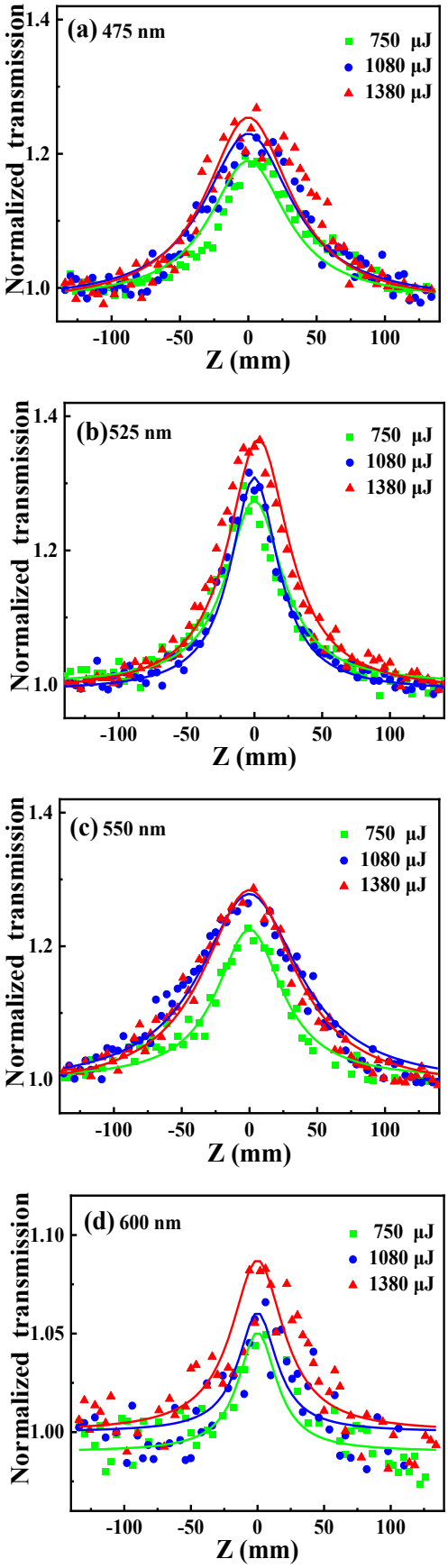

Fig. 2. The Z-scan curve of different wavelengths gold NPs (a) 475, (b) 525, (c) 550, and (d) 600 nm with different excited energies (color online)

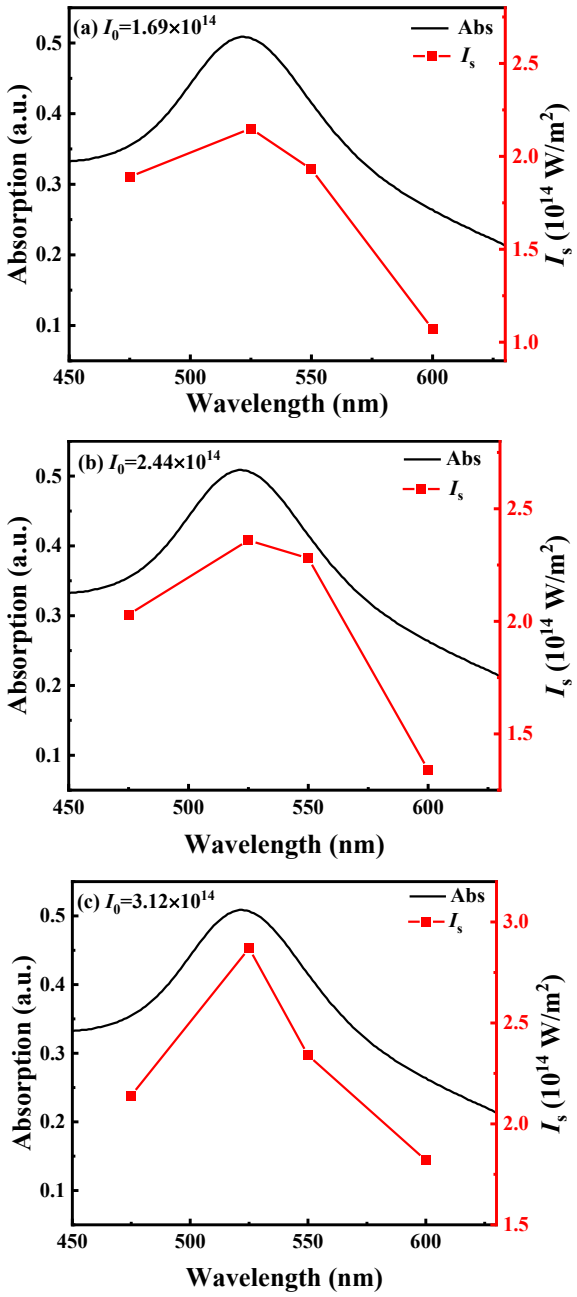

Fig. 3. The relationship between saturated light intensity and wavelengths (The solid lines are the linear absorption spectra). The dotted lines are saturation intensity. (a) when I_0 = 1.69×10^{14} W/m^2 (b) when I_0 =2.44×10^{14} W/m^2 (c) when I_0 =3.12×10^{14} W/m^2 (color online)

In the Fig. 3, we can intuitively observe the strong dependence of saturated intensity on excitation wavelength and SPR. In Figs. 3(a), (b) and (c), when the excitation wavelength is closer to the absorption peak, the saturation light intensity value is larger. It is because at the absorption peak (i.e., at the SPR resonance wavelength), a strong resonance between the free electrons and the incident light field significant enhances the local electric field, which makes more light energy is absorbed by the nanoparticles, leading to an increase in the number of ES electrons and a faster saturation of the absorptive capacity of the material. Therefore, the transmittance increases, leading to a higher saturated light intensity as the excitation wavelength approaches the absorption peak, resulting in stronger SA. Additionally, as the saturation intensity increases, the nonlinear resonance effect of the sample also increases [28]. Conversely, the saturated light intensity gradually decreases as the excitation wavelength moves away from the absorption peak. This is due to a combination of reduced absorption efficiency, weakened SPR effect and weakened NLO processes. This phenomenon has been observed in nonlinear measurements of gold nanostructures such as gold triangles, nanocages and nanorods [29-31].

In order to study the ultrafast carrier dynamic of 20 nm gold NPs, we used a pump-probe experiment for broadband TA spectroscopy [26]. Here, we investigated the ultrafast carrier dynamics at four different probe wavelengths using 400 nm as the pump wavelength. The pump-probe results of the gold NPs were selected for detection at 515, 525, 532 and 540 nm, respectively.

The normalized kinetic curves of gold NPs are shown in the Fig. 4(a), and the kinetic curves were numerically fitted. The fitted results exhibited a fast decreasing and decaying trend [32-34]. The rapid decline process is attributed to the large number of GS electrons being pumped into the ES of the system, resulting in GS bleaching and plasma formation, which is also known as electron-electron scattering. The decay processes are divided into fast and slow processes: the former is due to the electron-phonon relaxation process, resulting from the interaction between electrons and the crystal lattice, with a time scale of about a few picoseconds. The latter decay process is due to phonon-phonon relaxation process, caused by thermal effects produced by the high-speed motion of the crystal lattice, followed by the phonons spreading to the surrounding environment in the form of heat energy to cool down [35-40]. Since there are two kinds of decay processes, we use the double-exponential function to fit the dynamic curve [41]:

$$\frac{\Delta T}{T} = A_1 \exp\left(-\frac{t}{\tau_1}\right) + A_2 \exp\left(-\frac{t}{\tau_2}\right) \tag{5}$$

where A_1, A_2 and τ_1, τ_2 are the amplitudes and time constants of two decay components, respectively. In Fig. 4(a), we fitted the experimental data with a solid line to the equation to obtain the fast decay time τ_1 and slow recovery time τ_2, as shown in Table 2. It can see that the lifetime of the gold NPs decreases as the detection wavelength increases. This is because the decay time is related to the laser intensity during pumping, and the decay time increases significantly with the increase of the laser intensity. Nevertheless, as the detection wavelength becomes shorter, the more its photon energy increases.

Under high excitation energy, gold NPs have a higher initial temperature of thermionic electrons. Due to the thermal effect, there exists a temperature difference between electrons and phonons, altering the energy exchange mechanism within the system. With higher energy, it taken longer for the electronic to transfer energy to the phonon, resulting in a longer decay time.

The Fig. 4(b) shows the pump intensity of 4.05×10^3 mW/cm^2 and TA spectrum at five-time scales of 0, 1.3, 6.5, 13.7, and 134.5 ps. After the sample is excited, a GS bleaching signal of the plasma is generated at 525 nm. This occurs because a certain number of molecules in the GS are excited to the ES by the pumping pulse. When the sample is excited, the GS absorption of the probe light is less than that of an unexcited sample in the GS, resulting in a negative signal at 525 nm.

Table 1. Correlated NLO parameters of 20 nm gold NPs

λ (nm)	E (μJ)	I_0 ($\times10^{14}$ W/m^2)	I_s ($\times10^{14}$ W/m^2)
	750	1.69	1.89
475	1080	2.44	2.03
	1380	3.12	2.14
	750	1.69	2.15
525	1080	2.44	2.36
	1380	3.12	2.87
	750	1.69	1.93
550	1080	2.44	2.28
	1380	3.12	2.34
	750	1.69	1.07
600	1080	2.44	1.34
	1380	3.12	1.82

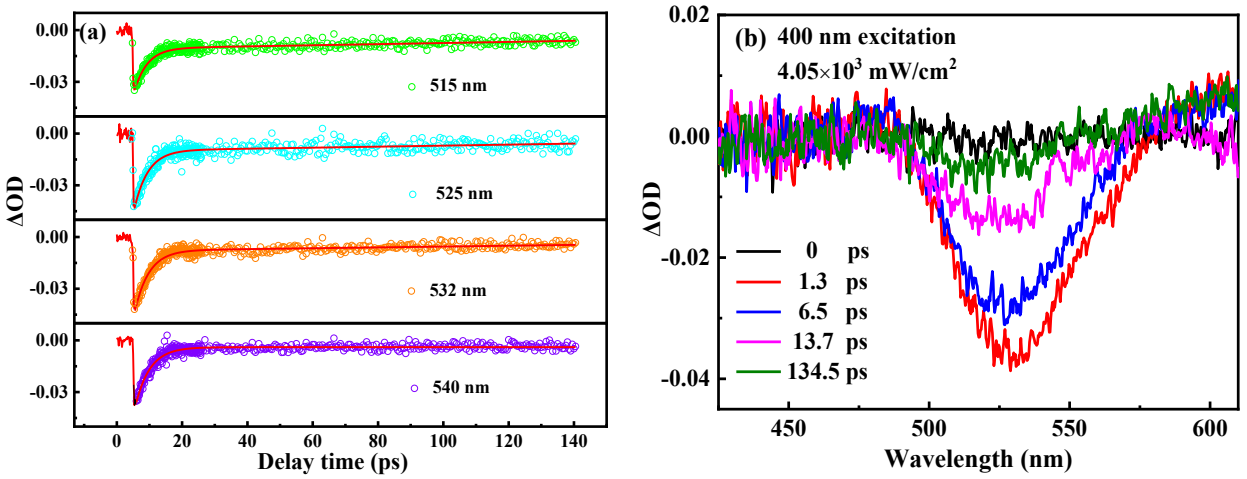

Fig. 4. (a) The TA kinetic curves and fitted curves at different probe wavelengths with pump intensity of 4.05×10^3 mW/cm^2. (b) The transient spectra of gold NPs at different delay times (color online)

Table 2. Correlated NLO parameters of 20 nm gold NPs

λ (nm)	τ_1 (ps)	τ_2 (ps)
515	0.009	5.061
525	0.068	5.365
532	0.010	5.153
540	0.064	4.607

Within the interval of 13.7 ps, the former time scale changes uniformly, and the recovery is faster; the latter time scale increases sharply, indicating relatively slow exciton recombination in gold NPs. To investigate the duration required to restore the original state, detections were conducted on larger time scales (134.5 ps). However, due to thermal effects, the original state did not coincide within the measured time scale. This is due to the fact that when gold NPs are irradiated with excitation light, the thermal effect results from this SPR effect that leads to an increase in the temperature of the medium surrounding the nanoparticles. At longer time scales (134.5 ps), this thermal accumulation effect becomes more pronounced, thus affecting the recovery process of the system.

4. Conclusion

In summary, in the OA Z-scan experiments, the 20 nm gold NPs exhibit SA under both multi-energies and multi-excitation wavelengths, with the sample has the highest saturation intensity in the resonance region, primarily due to GS bleaching. In addition, the interdependence between the saturation intensity and the excitation wavelength of the sample was observed,

meaning that as the excitation wavelength approaches the absorption peak, the saturation intensity increases. The ultrafast carrier dynamics of gold NPs involve both fast and slow processes. The fast process is caused by the electron-phonon coupling, while the slow process is attributed to the phonon-phonon coupling. The fast relaxation time is theoretically calculated at different wavelengths, revealing that the large energy transfer between particles leads to gold NPs having a higher initial temperature of hot electrons and a longer electron relaxation time. The above results provide deeper insights into the effects of absorption spectra of gold NPs and enhance our understanding of ultrafast laser-matter interactions. Moreover, these findings have potential applications in achieving the modulation of plasma resonance frequencies of metal NPs through spectral modulation and experimental measurement of a series of photophysical parameters such as saturation light intensity and response time of related materials. They offer important guidance and reference value for the development of future optoelectronic devices, including photocatalysis and medical therapy.

References

[1] C. Zheng, J. Huang, L. Lei, W. Chen, H. Wang, W. Li, Applied Physics B-Lasers and Optics **1**(124), 1 (2018).

[2] Y. Hua, K. Chandra, D. H. M. Dam, G. P. Wiederrecht, T. W. Odom, Journal of Physical Chemistry Letters **24**(6), 4904 (2015).

[3] I. Russier-Antoine, F. Bertorelle, M. Vojkovic, D. Rayane, E. Salmon, C. Jonin, P. Dugourd, R. Antoine, P.-F. Brevet, Nanoscale **22**(6), 13572 (2014).

[4] E. V. Garcia-Ramirez, S. Almaguer-Valenzuela, O. Sanchez-Dena, O. Baldovino-Pantaleon, J. A. Reyes-Esqueda, Optics Express **2**(24), A154 (2016).

[5] S. L. Smitha, K. G. Gopchandran, N. Smijesh, R. Philip, Progress in Natural Science-Materials International **1**(23), 36 (2013).

[6] H. Wang, X. Liu, X. Li, W. Lu, L. Jiang, ChemistrySelect **4**(1), 659 (2016).

[7] H. Lunden, A. Liotta, D. Chateau, F. Lerouge, F. Chaput, S. Parola, C. Brannlund, Z. Ghadyani, M. Kildemo, M. Lindgren, C. Lopes, Journal of Materials Chemistry C **5**(3), 1026 (2015).

[8] O. Sanchez-Dena, P. Mota-Santiago, L. Tamayo-Rivera, E. V. Garcia-Ramirez, A. Crespo-Sosa, A. Oliver, J. A. Reyes-Esqueda, Optical Materials Express **1**(4), 92 (2014).

[9] R. Rajaramakrishna, C. Saiyasombat, R. V. Anavekar, H. Jain, Journal of Non-Crystalline Solids **406**, 107 (2014).

[10] J. M. P. Almeida, D. S. da Silva, L. R. P. Kassab, S. C. Zilio, C. R. Mendonca, L. De Boni, Optical Materials **4**(36), 829 (2014).

[11] S. Link, M. A. El-Sayed, The Journal of Physical Chemistry B **21**(103), 4212 (1999).

[12] V. Amendola, R. Pilot, M. Frasconi, O. M. Marago, M. A. Iati, Journal of Physics-Condensed Matter. **20**(29), 203002 (2017).

[13] S. Afewerki, A. Cordova, Chemical Reviews **22**(116), 13512 (2016).

[14] S. Her, D. A. Jaffray, C. Allen, Advanced Drug Delivery Reviews **109**, 84 (2017).

[15] H. Tian, M. L. Chin, S. Najmaei, Q. Guo, F. Xia, H. Wang, M. Dubey, Nano Research **6**(9), 1543 (2016).

[16] J. Zhao, S. C. Nguyen, R. Ye, B. Ye, H. Weller, G. A. Somorjai, A. P. Alivisatos, F. D. Toste, ACS Central Science **5**(3), 482 (2017).

[17] C. Wang, X.-G. Nie, Y. Shi, Y. Zhou, J.-J. Xu, X.-H. Xia, H.-Y. Chen, ACS Nano **6**(11), 5897 (2017).

[18] L. Yan, F. Wang, S. Meng, ACS Nano **5**(10), 5452 (2016).

[19] J. Lee, S. Mubeen, X. Ji, G. D. Stucky, M. Moskovits, Nano Letters **9**(12), 5014 (2012).

[20] D. Peckus, A. Tamuleviciene, K. Mougin, A. Spangenberg, L. Vidal, Q. Bauerlin, M. Keller, J. Henzie, L. Puodziukynas, T. Tamulevicius, S. Tamulevicius, Optics Express **15**(30), 27730 (2022).

[21] U. Kreibig, L. Genzel, Surface Science Letters **part-P2**(156), 678 (1985).

[22] T. S. Ahmadi, S. L. Logunov, M. A. El-Sayed, The Journal of Physical Chemistry **20**(100), 8053 (1996).

[23] M. Sheik-Bahae, A. A. Said, T. H. Wei, IEEE Journal of Quantum Electronics **4**(26), 760 (1990).

[24] R. Fathima, A. Mujeeb, Journal of Alloys and Compounds **858**, 157667 (2021).

[25] J. Turkevich, P. C. Stevenson, J. Hillier, Discussions of the Faraday Society **11**, 55 (1951).

[26] A. M. Brown, R. Sundararaman, P. Narang, A. M. Schwartzberg, W. A. Goddard, III, H. A. Atwater, Physical Review Letters **118**, 087401 (2017).

[27] J. T. Seo, Q. Yang, W.-J. Kim, J. Heo, S.-M. Ma, J. Austin, W. S. Yon, S. S. Jung, S. W. Han, B. Tabibi, D. Temple, Optics Letters **3**(34), 307 (2009).

[28] L. Brus, Accounts of Chemical Research **12**(41), 1742 (2008).

[29] M. A. van der Veen, G. Rosolen, T. Verbiest, M. K. Vanbel, B. Maes, B. Kolaric, Journal of Materials Chemistry C **7**(3), 1576 (2015).

[30] S. Chen, S. Yang, Y. Huang, W. Jiao, G. Fan, Y. Gao, Chinese Optics Letters **1**(18), 011901 (2020).

[31] H.-M. Gong, Z.-K. Zhou, S. Xiao, H. Song, X.-R. Su, M. Li, Q.-Q. Wang, Chinese Physics Letters **12**(24), 3443 (2007).

[32] J. H. Hodak, I. Martini, G. V. Hartland, The Journal of Physical Chemistry B **36**(102), 6958 (1998).

[33] J. H. Hodak, A. Henglein, G. V. Hartland, The Journal of Chemical Physics **13**(112), 5942

(2000).
[34] S. Link, M. A. El-Sayed, T. G. Schaaff, R. L. Whetten, Chemical Physics Letters **3-4**(356), 240 (2002).
[35] M. L. Brongersma, N. J. Halas, P. Nordlander, Nature Nanotechnology **1**(10), 25 (2015).
[36] J. Saavedra, A. Asenjo-Garcia, F. J. García de Abajo, ACS Photonics **9**(3), 1637 (2016).
[37] G. V. Hartland, Chemical Reviews **6**(111), 3858 (2011).
[38] G. V. Hartland, Physical Chemistry Chemical Physics **23**(6), 5263 (2004).
[39] S. Link, C. Burda, Z. L. Wang, M. A. El-Sayed, The Journal of Chemical Physics **3**(111), 1255 (1999).
[40] Groeneveld, Sprik, Lagendijk, Physical Review B, Condensed Matter **17**(51), 11433 (1995).
[41] C. Chen, J. Wang, S. Yang, W. Wu, D. Kong, Y. Gao, Journal of Nanoparticle Research **9**(20), 242 (2018).

*Corresponding author: gaoyachen@hlju.edu.cn